



HAL
open science

Optimization of Energy Harvesting MISO Communication Channels

Rajeev Gangula, David Gesbert, Deniz Gunduz

► **To cite this version:**

Rajeev Gangula, David Gesbert, Deniz Gunduz. Optimization of Energy Harvesting MISO Communication Channels. 2014. hal-00974600v2

HAL Id: hal-00974600

<https://hal.science/hal-00974600v2>

Preprint submitted on 8 Apr 2014 (v2), last revised 20 Nov 2014 (v3)

HAL is a multi-disciplinary open access archive for the deposit and dissemination of scientific research documents, whether they are published or not. The documents may come from teaching and research institutions in France or abroad, or from public or private research centers.

L'archive ouverte pluridisciplinaire **HAL**, est destinée au dépôt et à la diffusion de documents scientifiques de niveau recherche, publiés ou non, émanant des établissements d'enseignement et de recherche français ou étrangers, des laboratoires publics ou privés.

Optimization of Energy Harvesting MISO Communication Channels

Rajeev Gangula, *Student Member, IEEE*, David Gesbert, *Fellow, IEEE*, and Deniz Gündüz,
Member, IEEE

Abstract

Optimization of a point-to-point multiple-input single-output (MISO) communication system is considered when both the transmitter (TX) and the receiver (RX) have energy harvesting (EH) capabilities. The RX is interested in feeding back the channel state to the TX to help improve the transmission rate. The objective is to maximize the throughput by a deadline, subject to the EH constraints at the TX and the RX. The throughput metric considered is an upper bound on the ergodic rate of MISO channel with beamforming and limited feedback. Feedback bit allocation and transmission policies that maximize an upper bound on the ergodic rate are obtained. Tools from majorization theory are used to simplify the formulated optimization problems. Optimal policies obtained for the modified problem outperform the naive scheme in which no intelligent management of energy is performed.

Index Terms

Energy harvesting, Limited feedback, MISO, Offline optimization.

I. INTRODUCTION

Powering up terminals in communication networks by renewable energy is a promising approach in at least two ways. The first and obvious advantage is that, it reduces the carbon footprint of the information and communication technologies, which can no longer be neglected with the exponential growth in the number of communication devices. The second reason is that it increases the autonomy of battery-run communication devices. In traditional wireless networks, nodes get their energy from the power grid by always or periodically connecting to it. While it is easy to connect the terminals to the grid in some

R. Gangula, D. Gesbert are with the Mobile Communications Dept., EURECOM, France (email: {gangula, gesbert}@eurecom.fr). D. Gunduz is with Dept. of Electrical and Electronic Engineering, Imperial College London, UK (email: d.gunduz@imperial.ac.uk). Part of this work was presented at GlobalSIP 2013 in Austin, U.S.A., [1].

networks, in others, such as sensor networks, it cannot be done once after the deployment. Therefore, in such networks a node's lifetime, and hence, the network lifetime, is constrained by the limited initial energy in the battery. Providing EH capabilities to the communication nodes is an attractive solution to the network lifetime problem [2]. An EH node can scavenge energy from the environment (typical sources are solar, wind, vibration, thermal, etc.) [3]. With EH nodes in the network, in principle, one can guarantee perpetual lifetime without the need of replacing batteries.

However, EH poses a new design challenge as the energy sources are typically sporadic and random. The main challenge lies in ensuring Quality of Service (QoS) constraints of the network given the random and time varying energy sources. This calls for the intelligent management of various parameters involved in a communication system.

Recently, a significant number of works have appeared studying the optimal transmission schemes for EH communication systems under different assumptions regarding the node's knowledge about the underlying EH process. Offline optimization framework deals with systems in which non-causal knowledge of the EH process is available. Within this frame work, optimal transmission schemes are studied for the point-to-point fading channel [4], broadcast channel [5], [6], [7] and relay channel [8]–[10]. Extensions, taking into account the imperfections in battery [7] as well as circuit power consumption [11], [12] are also investigated. See [13] for an extensive overview.

To the best of our knowledge, a common aspect of all prior works on EH communication networks is that the TX is assumed to have access to perfect CSI. Knowledge of the CSI at the TX is beneficial in designing the optimal channel adaptation techniques, TX filters in multi-antenna systems. However, recent studies have demonstrated that, although feedback enhances the system performance, feedback resources, namely power and bandwidth, are limited, and must be spent wisely [14]. As a result, an important question arises: How do the EH constraints affect the design of feedback enabled wireless networks?

In this paper, we study the optimization of a feedback enabled EH MISO channel, where feedback is used to improve the rate through array gain. In the first part of the paper, we consider the optimization of the feedback policy under EH constraints at the RX, while the TX is assumed to have a constant power supply. The motivation is to address the following: In the case of EH, the available energy at the RX varies over time. Should the RX feedback same quality of CSI at all times? If so, can the CSI feedback quality be improved by using more bandwidth in the low energy scenario? In the second part of this paper, we assume that both the TX and the RX harvest energy. In this case, the transmission power policy and the feedback policy are coupled, and need to be jointly optimized. Results from multivariate

majorization theory are used to devise simple algorithms.

The rest of the paper is organized as follows. In Section II, a brief preliminary description of majorization theory is given. Section III presents the system model and summarizes the main assumptions in this paper. In Section IV, the feedback optimization problem when only the RX harvests energy is considered. Section V deals with throughput optimization when both the TX and the RX harvest energy. Numerical results are presented in Section VI to validate the analysis. Finally, Section VII concludes the paper.

Notation: Matrices are represented by uppercase bold letters, vectors are represented by bold slant letters. The transpose and conjugate transpose of matrix \mathbf{A} is denoted by \mathbf{A}^T and \mathbf{A}^H , respectively. We use $\{\mathbf{D}\}_{i,j}$ to denote the element at the i -th row and j -th column of matrix \mathbf{D} , and $|\mathcal{S}|$ to denote the cardinality of the set \mathcal{S} . The set of integers from m to n , $m < n$, is represented by $[m : n]$. The notation $\|\mathbf{x}\|$ refers the Euclidean norm of the vector \mathbf{x} , and $\angle(\mathbf{x}, \mathbf{y})$ refers to the angle between vectors \mathbf{x} and \mathbf{y} . The algorithm with name ‘‘Algo’’ is represented as $[O_1, O_2, \dots, O_n] = \mathbf{Algo}(I_1, I_2, \dots, I_n)$, where I_1, I_2, \dots, I_n are input arguments and O_1, O_2, \dots, O_n are output arguments. Finally, a circularly-symmetric complex Gaussian distributed random variable η with zero mean and variance σ^2 is denoted by $\eta \sim \mathcal{CN}(0, \sigma^2)$.

II. PRELIMINARIES

In this section, the basic notion of majorization is introduced and some important results that are used in this work are stated. The readers are referred to [15] for a complete reference on this subject. Majorization theory formalizes the notion that the components of a vector \mathbf{x} are ‘‘less spread out’’ than the components of a vector \mathbf{y} .

Definition 1: Let $\mathbf{x} = [x_1, \dots, x_n]$, $\mathbf{y} = [y_1, \dots, y_n]$, $\mathbf{x}, \mathbf{y} \in \mathbb{R}^n$ and let $x_{(i)}$ denote the i -th largest component of \mathbf{x} . Then \mathbf{x} is said to be *majorized* by \mathbf{y} , denoted by $\mathbf{x} \preceq \mathbf{y}$, if

$$\begin{aligned} \sum_{i=1}^l x_{(i)} &\leq \sum_{i=1}^l y_{(i)}, & 1 \leq l < n, \\ \sum_{i=1}^n x_{(i)} &= \sum_{i=1}^n y_{(i)}. \end{aligned}$$

Definition 2: [15, 2.A.1] A $n \times n$ matrix \mathbf{D} with elements $\{\mathbf{D}\}_{i,j}$ is *doubly stochastic* if

$$\begin{aligned} \{\mathbf{D}\}_{i,j} &\geq 0, & \forall i, j \in [1 : n], \\ \sum_{i=1}^n \{\mathbf{D}\}_{i,j} &= 1, & \forall j \in [1 : n] \text{ and } \sum_{j=1}^n \{\mathbf{D}\}_{i,j} = 1, & \forall i \in [1 : n]. \end{aligned}$$

Theorem 1: [15, 4.A.1, 4.B.1] For $\mathbf{x}, \mathbf{y} \in \mathbb{R}^n$, the following conditions are equivalent:

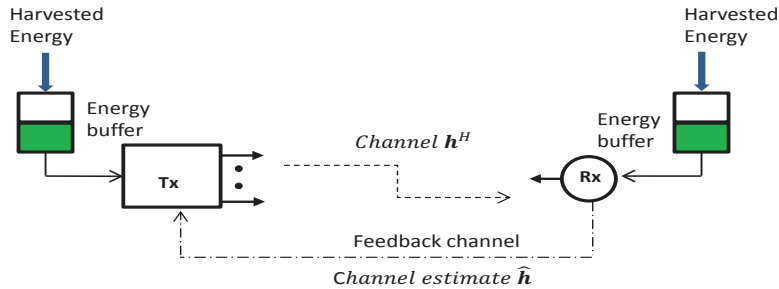


Figure 1. MISO channel with EH nodes.

- $\mathbf{x} \preceq \mathbf{y}$.
- $\mathbf{x} = \mathbf{y}\mathbf{D}$ for some doubly stochastic matrix \mathbf{D} .
- For all continuous concave functions $g : \mathbb{R} \rightarrow \mathbb{R}$, $\sum_{i=1}^n g(x_i) \geq \sum_{i=1}^n g(y_i)$.

Definition 3: [15, 15.A.2] Let \mathbf{X} and \mathbf{Y} be $m \times n$ real matrices. Then \mathbf{X} is said to be *majorized* by \mathbf{Y} , written $\mathbf{X} \preceq \mathbf{Y}$, if $\mathbf{X} = \mathbf{Y}\mathbf{D}$, where the $n \times n$ matrix \mathbf{D} is doubly stochastic.

Theorem 2: [15, 15.A.4] Let \mathbf{X} and \mathbf{Y} be $m \times n$ real matrices. Then, $\mathbf{X} \preceq \mathbf{Y}$ if and only if

$$\sum_{i=1}^n g(\mathbf{x}_i^c) \geq \sum_{i=1}^n g(\mathbf{y}_i^c),$$

for all continuous concave functions $g : \mathbb{R}^m \rightarrow \mathbb{R}$, where \mathbf{x}_i^c and \mathbf{y}_i^c denotes the i -th column vector of \mathbf{X} and \mathbf{Y} , respectively.

III. SYSTEM MODEL

We consider a point-to-point MISO fading channel as shown in Fig. 1, where both the TX and the RX harvest energy from the environment. Each node is equipped with an individual energy buffer, i.e., a rechargeable battery, that can store the locally harvested energy.

A. Energy Harvesting Model

The total observation time is divided into K equal length EH intervals. At the beginning of the k -th EH interval, $k \in [1 : K]$, new energy packets of size E_k^t, E_k^r units arrive at the TX and the RX, respectively. At each node, this energy is first stored in an infinite size energy buffer, and used only for communication purposes, i.e., TX sending data to the RX, and the RX feeding back the CSI. We assume that all E_k^t, E_k^r 's

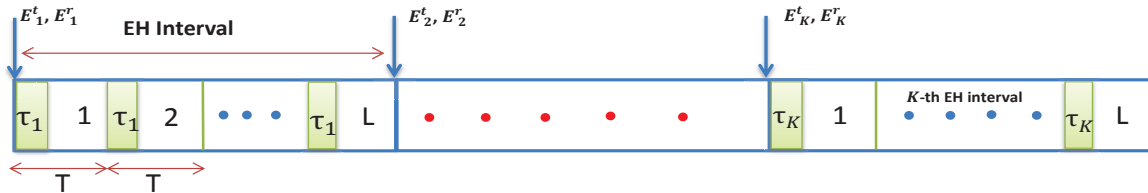


Figure 2. Energy harvesting time frame structure.

are known in advance by both terminals. This model is suitable for an EH system in which the amount of harvested energy can be predicted in advance.

B. Communication System Model

Each EH interval consists of L data frames, each of length T channel uses. We assume a block fading channel model. The channel is constant during T channel uses of each frame, but changes in an independent and identically distributed (i.i.d) fashion from one frame to another. The time frame structure is shown in Fig. 2. The TX has $M > 1$ antennas. The received signal in a given channel use is given by

$$y = \mathbf{h}^H \mathbf{w} s + \eta, \quad (1)$$

where $\mathbf{h} \in \mathbb{C}^{M \times 1}$ represents the vector of channel coefficients from TX antenna array to the RX with i.i.d $\mathcal{CN}(0, 1)$ elements, $\mathbf{w} \in \mathbb{C}^{M \times 1}$ denotes the unit norm beamforming vector, the input symbol maximizing the achievable ergodic rate in the k -th EH interval is $s \sim \mathcal{CN}(0, P_k)$, and $\eta \sim \mathcal{CN}(0, 1)$ represents the noise at the RX.

C. Feedback Model

We assume that the RX perfectly estimates the channel state at the beginning of each data frame, and feeds back the quantized CSI to the TX within the same frame. In the k -th EH interval, the frame structure is as follows: The RX in τ_k channel uses sends the CSI through a feedback channel (uplink) which is modeled as additive white Gaussian noise (AWGN) channel. In the remaining $T - \tau_k$ channel uses, TX sends data to the RX (downlink) exploiting the obtained CSI. The feedback model represents the Time-Division Duplex (TDD) system in which uplink and downlink use the same band in a time-sharing

fashion, but the communication devices are not self-calibrated and hence induce non-reciprocal effects [16], [17]. In the above model, although the feedback overhead incurs cost in the downlink bandwidth, similar trade-off in resource allocation between the CSI feedback quality and uplink data rate also arise in a Frequency-Division Duplex (FDD) system. Analytical results obtained in this paper are applicable in general settings, and for instance, can be used to address the trade-off between CSI quality and effective data rate in a FDD system.

In the k -th EH interval, quantization of the channel state is performed using a codebook C_k known at both the TX and RX. The receiver uses Random Vector Quantization (RVQ). The codebook consists of M -dimensional unit vectors $C_k \triangleq \{\mathbf{w}_1, \dots, \mathbf{w}_{2^{B_k}}\}$, where B_k is the number of bits used for quantization. The RX computes the quantization index according to $\hat{\mathbf{h}} = \arg \max_{\mathbf{w} \in C_k} |\tilde{\mathbf{h}}^H \mathbf{w}|^2$, where $\tilde{\mathbf{h}} \triangleq \frac{\mathbf{h}}{\|\mathbf{h}\|}$. We assume that the length of the EH interval is very large compared to the channel coherence time (i.e., L is very large). As a result, the achievable ergodic rate in the k -th EH interval is given by

$$R_k = \left(1 - \frac{\tau_k}{T}\right) E_{\mathbf{h}, \mathcal{W}} \left[\log_2 \left(1 + \frac{P_k}{\left(1 - \frac{\tau_k}{T}\right)} \|\mathbf{h}\|^2 \cos^2 \left(\angle(\tilde{\mathbf{h}}, \hat{\mathbf{h}}) \right) \right) \right]. \quad (2)$$

By using the AWGN feedback channel model, the number of feedback bits B_k can be related to the energy used by the RX, Q_k , and the number of channel uses τ_k as follows:

$$B_k = \tau_k \log_2 \left(1 + \frac{Q_k}{\tau_k \sigma^2} \right), \quad (3)$$

where σ^2 is the noise variance in the uplink. For analytical tractability, we neglect the practical constraint that B_k should be an integer. Using the ergodic rate expression given in [18, (27)] and (3), the ergodic rate $R_k \triangleq R(P_k, Q_k, \tau_k)$ is given by

$$R_k = \left(1 - \frac{\tau_k}{T}\right) \log_2 e \left(e^{\left(\frac{1 - \frac{\tau_k}{T}}{P_k}\right)} \sum_{l=0}^{M-1} E_{l+1} \left(\frac{1 - \frac{\tau_k}{T}}{P_k} \right) - \int_{\nu=0}^1 \left(1 - (1 - \nu)^{M-1}\right) \left(1 + \frac{Q_k}{\tau_k \sigma^2}\right)^{\tau_k} \frac{M}{\nu} e^{\left(\frac{1 - \frac{\tau_k}{T}}{P_k \nu}\right)} E_{M+1} \left(\frac{1 - \frac{\tau_k}{T}}{P_k \nu} \right) d\nu \right), \quad (4)$$

where $E_n(\cdot)$ is the n -th order exponential integral.

D. Optimization Problem

The problem of maximizing the sum throughput by the end of the K -th EH interval can be formulated as

$$\max_{P_k, Q_k, \tau_k} \sum_{k=1}^K R_k \quad (5a)$$

$$\text{s.t.} \quad L \sum_{i=1}^l Q_i \leq \sum_{i=1}^l E_i^r, \quad l = 1, \dots, K, \quad (5b)$$

$$LT \sum_{i=1}^l P_i \leq \sum_{i=1}^l E_i^t, \quad l = 1, \dots, K, \quad (5c)$$

$$0 \leq \tau_k < T, \quad P_k \geq 0, \quad \text{and} \quad Q_k \geq 0, \quad k = 1, \dots, K. \quad (5d)$$

The constraints (5b) and (5c) are known as *energy neutrality constraints*, represent the fact that, at each node, the energy consumed can not be more than the energy harvested till that time. Before tackling the above problem, first, we consider a special case in which only the RX harvests energy. In this scenario, the aim is to obtain the optimal feedback policy under the EH constraints at the RX. Latter, the general case with both the TX and the RX harvesting energy is studied.

IV. EH RECEIVER

In this setting, the RX harvests energy from the environment, whereas the TX is connected to the power grid so that it has a fixed power supply at all times. Therefore, there are no EH constraints at the TX, and constraints (5c) can be ignored. However, there is now a constraint on the average transmission power at each data frame of the k -th EH interval i.e., $P_k \leq P, \forall k$.

The ergodic rate expression in (4) offers little insight into the convexity of the problem which is required to reduce the complexity of optimization. This motivates the use of a bound on the ergodic rate as an objective function. By using the bound on the expected quantization error [19],

$$\mathbb{E}_{\mathcal{W}} \cos^2 \left(\angle(\tilde{\mathbf{h}}, \hat{\mathbf{h}}) \right) \leq 1 - \left(\frac{M-1}{M} \right) 2^{\frac{-B_k}{M-1}}, \quad (6)$$

and the Jensen's inequality, an upper bound on the ergodic rate $R_k^u \triangleq R^u(P_k, Q_k, \tau_k)$ is given by,

$$R_k^u = \left(1 - \frac{\tau_k}{T} \right) \log_2 \left[1 + \frac{P_k M}{\left(1 - \frac{\tau_k}{T} \right)} \left(1 - \left(\frac{M-1}{M} \right) 2^{\frac{-B_k}{M-1}} \right) \right]. \quad (7)$$

From (3) and (7), the ergodic rate upper bound is expressed as

$$R_k^u = \left(1 - \frac{\tau_k}{T} \right) \log_2 \left[1 + \frac{P_k M}{\left(1 - \frac{\tau_k}{T} \right)} \left(1 - \frac{M-1}{M} \left(1 + \frac{Q_k}{\tau_k \sigma^2} \right)^{\frac{-\tau_k}{M-1}} \right) \right]. \quad (8)$$

The modified optimization problem is as follows,

$$\max_{P_k, Q_k, \tau_k} \quad \mathcal{U} = \sum_{k=1}^K R_k^u \quad (9a)$$

$$\text{s.t.} \quad L \sum_{i=1}^l Q_i \leq \sum_{i=1}^l E_i, l = 1, \dots, K, \quad (9b)$$

$$P_k \leq P, \quad \text{and} \quad P_k \geq 0, \quad k = 1, \dots, K, \quad (9c)$$

$$0 \leq \tau_k < T, \quad \text{and} \quad Q_k \geq 0, \quad k = 1, \dots, K, \quad (9d)$$

where P is the power constraint at the transmitter.

As the objective function is monotonic in Q_k and P_k , the constraint in (9b) must be satisfied with equality for $l = K$, the first constraint in (9c) must be satisfied with equality for $k \in [1 : K]$, otherwise, we can always increase Q_K, P_k , and hence the objective function, without violating any constraints. Therefore we can replace the variable P_k by letting $P_k = P, \forall k$. Now it remains to optimize over the variables Q_k and τ_k .

The feasible set is represented as

$$\mathfrak{F} = \{ \mathbf{Q}, \boldsymbol{\tau} \mid Q_k, \tau_k \text{ satisfy (9b), (9d)} \}, \quad (10)$$

where $\mathbf{Q} = [Q_1, \dots, Q_K]$ and $\boldsymbol{\tau} = [\tau_1, \dots, \tau_K]$. To show that the above problem is a convex optimization problem, we make use of the following lemma.

Lemma 1: If the function $f(x, t) : \mathbb{R}_+^2 \rightarrow \mathbb{R}_+$ is concave, and $g(y, z) : \mathbb{R}_+^2 \rightarrow \mathbb{R}_+$ is concave and monotonically increasing in each argument, then the function $h(x, y, t) = \left(1 - \frac{t}{T}\right) g\left(\frac{y}{1 - \frac{t}{T}}, \frac{f(x, t)}{1 - \frac{t}{T}}\right)$ is concave $\forall (x, y) \in \mathbb{R}_+^2, t \in [0, T]$.

Proof: The proof is similar to that of showing the perspective of a concave function is concave. See Appendix. ■

Proposition 1: The objective function in optimization problem (9) is concave.

Proof: See Appendix. ■

Since the objective function in (9) is concave and the constraints are linear, it has a unique maximizer [20]. Using the concavity of the objective function, we show that the optimal energy allocation vector is the most majorized feasible energy vector.

Proposition 2: The global optimum of (9) is obtained at $(\mathbf{Q}^*, \boldsymbol{\tau}^*)$, where $\mathbf{Q}^* \preceq \mathbf{Q}, \forall (\mathbf{Q}, \boldsymbol{\tau}) \in \mathfrak{F}$, and τ_k^* is the solution of the following equation

$$\frac{\partial R_k^u}{\partial \tau_k} \Big|_{(Q_k^*, \tau_k^*)} = 0, \quad \forall k \in [1 : K]. \quad (11)$$

Proof: Consider the following equivalent form of (9), where the optimization is performed in two steps.

$$\max_{\mathbf{Q}} \tilde{\mathcal{U}}(\mathbf{Q}) \text{ s.t. } \forall (\mathbf{Q}, \boldsymbol{\tau}) \in \mathfrak{F}, \quad (12)$$

where $\tilde{\mathcal{U}}(\mathbf{Q})$ is obtained by

$$\tilde{\mathcal{U}}(\mathbf{Q}) = \max_{\boldsymbol{\tau}} \mathcal{U}(\mathbf{Q}, \boldsymbol{\tau}) \text{ s.t. } \forall (\mathbf{Q}, \boldsymbol{\tau}) \in \mathfrak{F}. \quad (13)$$

Since \mathcal{U} is a concave function over the convex set \mathfrak{F} , the function $\tilde{\mathcal{U}}(\mathbf{Q})$ is concave, where the domain of $\tilde{\mathcal{U}}$ is the set $\tilde{\mathfrak{F}} = \{\mathbf{Q} | (\mathbf{Q}, \boldsymbol{\tau}) \in \mathfrak{F}\}$ [20, 3.2.5]. $\mathcal{U} = \sum_{k=1}^K R_k^u$ is continuous, differentiable and concave in $\tau_k \in [0, T)$. Furthermore, for given Q_k , R_k^u approaches $\log_2(1+P)$ and 0 as τ_k approaches 0 and T , respectively. Therefore, the unique maximizer of (13) lies in $[0, T)$ and it is obtained at

$$\frac{\partial \mathcal{U}}{\partial \tau_k} \Big|_{\tau_k^*} = \frac{\partial R_k^u}{\partial \tau_k} \Big|_{\tau_k^*} = 0, \quad \forall k \in [1 : K]. \quad (14)$$

From above, as τ_k^* is only a function of Q_k ,

$$\tilde{\mathcal{U}}(\mathbf{Q}) = \sum_{k=1}^K \tilde{R}_k^u \quad (15)$$

where $\tilde{R}_k^u \triangleq \tilde{R}^u(Q_k) = R^u(Q_k, \tau_k^*(Q_k))$. Using (15) and Theorem 1, $\tilde{\mathcal{U}}(\mathbf{Q}^*) \geq \tilde{\mathcal{U}}(\mathbf{Q}), \forall \mathbf{Q} \in \tilde{\mathfrak{F}}$. Finding the optimal energy allocation vector \mathbf{Q}^* under the energy harvesting constraints turns out to be a well known problem, and the algorithm to construct \mathbf{Q}^* is given in various works [21]–[23]. The proof that the algorithm constructs the most majorized feasible energy vector is given in [23]. Since the optimal energy allocation vector is \mathbf{Q}^* , the optimal $\boldsymbol{\tau}^*$ is obtained by (11). ■

A brief description of the algorithm tailored to this work is given here, details can be found in [21]–[23]. Note that there is no closed form expression for the solution of (11), therefore we use numerical methods to obtain $\boldsymbol{\tau}^*$.

A. Optimal Energy Allocation

The Optimal Energy Allocation (**OEA**) algorithm, given in Algorithm 1, divides the EH intervals into $|\mathcal{S}|$ energy bands whose indices form the set $\mathcal{S} = \{t_0, t_1, \dots, t_{|\mathcal{S}|}\}$, where $t_i < t_j, \forall i < j$, $t_0 = 0$, and $t_{|\mathcal{S}|} = K$. The i -th energy band contains the EH intervals with indices $k \in [t_{i-1} + 1 : t_i]$. Moreover, the optimal allocated energy in each EH interval belonging to the i -th energy band is equal and it is denoted by $Q_{(i)}^*$. The energy vector \mathbf{Q}^* obtained by $[\mathbf{Q}^*, \mathcal{S}_r] = \mathbf{OEA}(K, \{E_i^r/L\})$, has the following properties:

(P1) $Q_k^* = Q_{(i)}^* = \frac{\sum_{l=t_{i-1}+1}^{t_i} E_l^r}{L(t_i - t_{i-1})}, \quad \forall k \in [t_{i-1} + 1 : t_i]$.

(P2) The entries $Q_{(i)}^*$ are strictly monotonic, i.e., $Q_{(1)}^* < Q_{(2)}^* < \dots < Q_{(|\mathcal{S}|)}^*$.

```

Input : Number of EH intervals  $K$ ; Harvested energy  $\{H_i\}$ 
Output: Energy allocation  $O^*$ , Energy band indices  $\mathcal{S} = \{t_0, t_1, \dots, t_{|\mathcal{S}|}\}$ 

// initialization
 $t_0 := 0$ ;

for  $i = 1 : K$  do
  for  $k = K : -1 : (t_{i-1} + 1)$  do
    (i)  $O_l^* = \frac{\sum_{j=t_{i-1}+1}^k H_j}{k-t_{i-1}}$ ,  $l \in \{t_{i-1} + 1, \dots, k\}$ 
    if  $\sum_{i=1}^l O_i^* \leq \sum_{i=1}^l H_i$ ,  $l = 1, \dots, K$  then
       $t_i := k$ ;
      Save  $\{O_1^*, \dots, O_k^*\}$ 
      break;
    end
  end
  if  $t_i = K$  then
    break;
  end
end

```

Algorithm 1: Optimal Energy Allocation (**OEA**)

V. EH TRANSMITTER AND RECEIVER

In this section, we consider the general case where both the TX and the RX harvest energy. The ergodic rate upper bound in (8) is not concave, but concave in each variable given the other variables are fixed. One standard approach is to apply an iterative optimization, known as block coordinate descent (BCD) method, which is known to converge to the local maximum if the problem is of the form

$$\max_{\mathbf{x}} f(x_1, x_2, \dots, x_n) \quad \text{s.t. } \mathbf{x} \in \mathcal{X}, \quad (16)$$

f is continuously differentiable over \mathcal{X} , which can be written as the Cartesian product of the sets $\mathcal{X}_1, \dots, \mathcal{X}_n$. Further, for each block i and $\mathbf{x} \in \mathcal{X}$, the maximum

$$\max_{\xi} f(x_1, \dots, x_{i-1}, \xi, x_{i+1}, \dots, x_n) \quad \text{s.t. } \xi \in \mathcal{X}_i, \quad (17)$$

exists and it is unique [24, 2.7.1]. The optimization problem in (9) with extra EH constraints at the TX in (5c), has the structure given in (16) and satisfies the condition in (17). Therefore, we can use the BCD

algorithm to find the transmission power and feedback policy. However, the algorithm is computationally intensive. To obtain a simple algorithm, we follow similar approach as in the previous section, and use a concave upper bound on (8) as the objective function for throughput optimization.

An upper bound $R_k^{ub} \triangleq R^{ub}(P_k, Q_k, \tau_k)$ is given by

$$R_k^{ub} = \left(1 - \frac{\tau_k}{T}\right) \log_2 \left[1 + \frac{\left(1 - \frac{\tau_k}{T} + P_k\right)}{\left(1 - \frac{\tau_k}{T}\right)^2} \left(M - (M-1) \left(1 + \frac{Q_k}{\tau_k \sigma^2}\right)^{\frac{-\tau_k}{M-1}} \right) \right]. \quad (18)$$

We now illustrate the tightness of the upper bound in (18) in the low and high power regimes. Let $t_k \triangleq 1 - \frac{\tau_k}{T}$ and $f_k \triangleq M - (M-1) \left(1 + \frac{Q_k}{\tau_k \sigma^2}\right)^{\frac{-\tau_k}{M-1}}$. For all feasible τ_k, P_k and Q_k , we can see that $0 < t_k \leq 1$ and $1 \leq f_k \leq M$. Consider

$$\begin{aligned} R_k^{ub} - R_k^u &= t_k \log_2 \left(1 + \left(1 + \frac{P_k}{t_k}\right) \frac{f_k}{t_k} \right) - t_k \log_2 \left(1 + \frac{P_k f_k}{t_k} \right) \\ &= t_k \log_2 \left(\frac{t_k^2 + t_k f_k + P_k f_k}{t_k + P_k f_k} \right) - t_k \log_2 (t_k) \end{aligned} \quad (19)$$

Note that (19) is decreasing in P_k for fixed τ_k and Q_k . Since τ_k, f_k are bounded, for fixed τ_k and Q_k at low SNR,

$$\begin{aligned} \lim_{P_k \rightarrow 0} R_k^{ub} - R_k^u &= t_k \log_2 \left(1 + \frac{f_k}{t_k} \right), \\ &\leq \log_2 (1 + M). \end{aligned} \quad (20)$$

For fixed τ_k and Q_k at high SNR,

$$\begin{aligned} \lim_{P_k \rightarrow \infty} R_k^{ub} - R_k^u &= -t_k \log_2 (t_k), \\ &\leq 0.5. \end{aligned} \quad (21)$$

From the above analysis, it can be seen that, (19) decreases as the power is increased, and bounded by a constant in the high power regime.

By using (18), the modified throughput maximization problem is formulated as

$$\max_{P_k, Q_k, \tau_k} \mathcal{U}_1 = \sum_{k=1}^K R_k^{ub} \quad (22a)$$

$$\text{s.t.} \quad L \sum_{i=1}^l Q_i \leq \sum_{i=1}^l E_i^r, \quad l = 1, \dots, K, \quad (22b)$$

$$LT \sum_{i=1}^l P_i \leq \sum_{i=1}^l E_i^t, \quad l = 1, \dots, K, \quad (22c)$$

$$0 \leq \tau_k < T, \quad P_k \geq 0, \quad \text{and} \quad Q_k \geq 0, \quad k = 1, \dots, K. \quad (22d)$$

Since the objective function is monotonic in Q_k and P_k , the constraints in (22b) and (22c) must be satisfied with equality for $l = K$, otherwise, we can always increase Q_K, P_K , and hence the objective function, without violating any constraints. The feasible set is represented as,

$$\tilde{\mathcal{J}} = \{(\mathbf{P}, \mathbf{Q}, \boldsymbol{\tau}) \mid P_k, Q_k, \tau_k \text{ satisfy (22b), (22c) and (22d)}\}, \quad (23)$$

where $\mathbf{P} = [P_1, \dots, P_K]$, $\mathbf{Q} = [Q_1, \dots, Q_K]$ and $\boldsymbol{\tau} = [\tau_1, \dots, \tau_K]$.

Proposition 3: The objective function in optimization problem (22) is concave.

Proof: See Appendix. ■

Since the objective function in (22) is concave and the constraints are linear, it has a unique maximizer [20]. Consider the following equivalent form of (22), where the optimization is performed in two steps.

$$\max_{\mathbf{P}, \mathbf{Q}} \tilde{\mathcal{U}}_1(\mathbf{P}, \mathbf{Q}) \quad \text{s.t. } \forall (\mathbf{P}, \mathbf{Q}, \boldsymbol{\tau}) \in \tilde{\mathcal{J}}, \quad (24)$$

where $\tilde{\mathcal{U}}_1(\mathbf{P}, \mathbf{Q})$ is obtained by

$$\tilde{\mathcal{U}}_1(\mathbf{P}, \mathbf{Q}) = \max_{\boldsymbol{\tau}} \mathcal{U}_1(\mathbf{P}, \mathbf{Q}, \boldsymbol{\tau}) \quad \text{s.t. } \forall (\mathbf{P}, \mathbf{Q}, \boldsymbol{\tau}) \in \tilde{\mathcal{J}}. \quad (25)$$

Since \mathcal{U}_1 is a concave function over the convex set $\tilde{\mathcal{J}}$, the function $\tilde{\mathcal{U}}_1$ is concave with domain $\tilde{\mathcal{J}} = \{(\mathbf{P}, \mathbf{Q}) \mid (\mathbf{P}, \mathbf{Q}, \boldsymbol{\tau}) \in \tilde{\mathcal{J}}\}$ [20, 3.2.5]. $\mathcal{U}_1 = \sum_{k=1}^K R_k^{ub}$ is continuous, differentiable and concave in $\tau_k \in [0, T)$. Furthermore, for given P_k and Q_k , R_k^{ub} approaches $\log_2(2 + P_k)$ and 0 as τ_k approaches 0 and T , respectively. Therefore, the unique maximizer of (25), $\tau_k^*, \forall k$ lies in $[0, T)$, and it is obtained at

$$\left. \frac{\partial \mathcal{U}_1}{\partial \tau_k} \right|_{\tau_k^*} = \left. \frac{\partial R_k^{ub}}{\partial \tau_k} \right|_{\tau_k^*} = 0, \quad \forall k \in [1 : K]. \quad (26)$$

As τ_k^* is only a function of Q_k and P_k , (24) can be written as

$$\max_{P_k, Q_k} \tilde{\mathcal{U}}_1 = \sum_{k=1}^K \tilde{R}_k^{ub} \quad \text{s.t. } \forall k, (P_k, Q_k) \in \tilde{\mathcal{J}}, \quad (27)$$

where $\tilde{R}_k^{ub} \triangleq \tilde{R}^{ub}(P_k, Q_k) = R^{ub}(P_k, Q_k, \tau_k^*(P_k, Q_k))$.

In order to get an insight on how the optimal solution of (24) may look like, consider a simple scenario in which there is only a sum power constraint at the TX and the RX, i.e., the constraints in (22b), (22c) has to be satisfied for only $l = K$. In this case, by Jensen's inequality, the uniform power allocation at the TX and the RX is optimal ¹. However, due to the EH constraints, this may not be feasible. Using this intuition, we can see that the optimal policy tries to equalize the powers as much as possible, while satisfying the EH constraints.

¹In this section, with slight abuse of terminology we use the terms RX power and RX energy interchangeably.

First, we consider the case where the EH profiles at the TX and the RX are similar and show that the optimization problem is considerably simplified.

A. Similar EH Profiles

The EH profiles are similar in the sense that the most majorized feasible vectors obtained from the EH profiles of the TX and RX, \mathbf{P}^* and \mathbf{Q}^* , have same structure, i.e., if $P_i^* = c_1, \forall i \in [m : n]$, then $Q_i^* = c_2, \forall i \in [m : n]$ for some constants $c_1, c_2 \geq 0$. We now give a formal definition.

Definition 4: By using the **OEA** algorithm, let $[\mathbf{Q}^*, \mathcal{S}_r] = \mathbf{OEA}(K, \{E_i^r/L\})$ and $[\mathbf{P}^*, \mathcal{S}_t] = \mathbf{OEA}(K, \{E_i^t/LT\})$. EH profiles at the TX and the RX are said to be similar if $\mathcal{S}_r = \mathcal{S}_t$.

In the case where only the RX is harvesting energy, the optimal energy allocation vector is the most majorized feasible energy vector, and it is obtained by using the OEA algorithm. The algorithm essentially try to make the energy vector as equalized as possible, while satisfying the EH constraints. From section II, we can see that the definition of majorization for the vector case does not directly extend to the matrix case. If OEA algorithm is used at the TX and RX separately, we get the most individually majorized power vectors, which in general may not be the optimal solution of (24). However, we now show that if the EH profiles are similar, the above mentioned approach is indeed optimal.

Proposition 4: If the EH profiles at the TX and the RX are similar then $(\mathbf{Q}^*, \mathbf{P}^*, \boldsymbol{\tau}^*)$ is the global optimum of (22), where $\mathbf{Q}^* \preceq \mathbf{Q}, \mathbf{P}^* \preceq \mathbf{P}, \forall (\mathbf{Q}, \mathbf{P}, \boldsymbol{\tau}) \in \mathfrak{J}$, and τ_k^* is the solution of

$$\frac{\partial R_k^{ub}}{\partial \tau_k} \Big|_{(P_k^*, Q_k^*, \tau_k^*)} = 0, \quad \forall k \in [1 : K]. \quad (28)$$

Proof: See Appendix. ■

B. Different EH Profiles

Unfortunately, we could not find a simple algorithm to solve (22) in a general setting where the EH profiles are not similar. In (27), if one variable is fixed, optimizing over the other variable has a *directional water-filling* interpretation [4], however, the difficulty lies in the fact that there is no closed form expression for \tilde{R}_k^{ub} . Nonetheless, using convexity of the objective function, some properties of the optimal solution are given below.

Lemma 2: Under the optimal policy, the transmission power P_k , and the energy used to send the feedback Q_k are non-decreasing in $k, \forall k \in [1 : K]$.

Lemma 3: Under the optimal policy, at the instants where R^{ub} changes, the energy buffer of either the TX or the RX is emptied.

The proofs of the above lemmas are given in Appendix.

VI. RESULTS

In this section, numerical results are obtained for a MISO system with the assumptions described in the system model. We start by a small note on how the results obtained by solving the optimization problems are used to evaluate the bounds on the throughput. Throughout the paper, due to the intractability and non-convexity of the exact ergodic rate expression in (4), upper bounds on (4) are used as the objective function in the formulated optimization problems. Hence, solving these modified optimization problems gives an upper bound on the throughput. Since the constraints in the original and the modified problem are kept same, the solution obtained for the modified optimization problem is also feasible in the original problem, and if used in evaluating the exact ergodic rate expression in (4), we get a lower bound on the throughput.

First, we compare different feedback bit allocation schemes when the RX harvests energy, while the TX has constant power supply. We assume that the RX is equipped with a solar EH device. Following [25], solar irradiance data is taken from the database reported in [26]. Each EH interval is of duration $\Delta = 1$ hour, $T = 200$ ms, resulting in $L = 18000$ frames.

The harvested power from the irradiance data can be calculated as, $P_{harv} = I[\text{Watt}/m^2] \times Area[m^2] \times \rho$, where ρ is the efficiency of the harvester. A hypothetical solar panel of variable area is assumed. The area of the panel is adjusted such that we have the EH profile shown in Fig. 3 at the RX. In Fig. 3, the harvested power to noise ratio (HPN) in each EH interval $\frac{E_k^r}{\Delta\sigma^2}$ is shown. Fig. 4 shows the throughput for different downlink signal to noise ratios (SNRs), with $M = 4$ antennas. In Fig. 4, OEA represents the proposed policy in which the energy vector is obtained by using the OEA algorithm. In the greedy scheme, optimization is performed only over τ , given $Q_k = E_k^r/L$. In Fig. 5, feedback bit allocation is shown for the above mentioned policies for a downlink SNR of 10 dB, with $M = 4$ antennas. From Fig. 5, we can see that the proposed feedback bit allocation is equalized as much as possible, i.e., follows the majorization property.

We now consider the case when both the TX and the RX harvest energy, and their EH profiles are similar. The TX and RX are equipped with a solar EH device. The same EH profile in Fig. 3 is used at both the RX and the TX. However, the mean HPN at the TX is varied by increasing the harvester area at the TX, i.e., the EH profile is multiplied by a positive number (area), while keeping the same shape. Fig. 6 shows the throughput for different mean HPN at the TX, with $M = 4$. In the greedy scheme, optimization is performed only over τ given $Q_k = E_k^r/L$ and $P_k = E_k^t/LT$. In Fig. 6, BCD represents the iterative optimization algorithm, and OEA represents the proposed policy in which the energy vectors

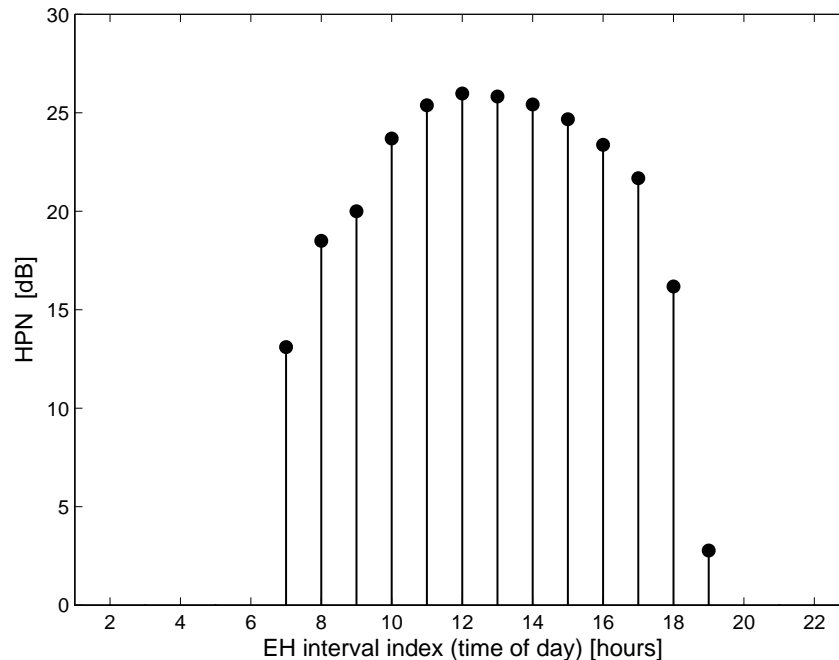


Figure 3. Model for solar energy harvesting profile.

are obtained by using the OEA algorithm. We can see that both OEA and BCD have similar performance, however, BCD is computationally intensive. The difference in throughput between the greedy and OEA is small when the average HPN is low, and it increases with increasing the HPN. In contrast to the OEA power allocation algorithm/scheme, using the greedy approach with the solar EH profile results in some EH intervals being allocated zero energy, and therefore does not scale by increasing the harvester area. This particularly hurts the greedy policy's throughput in the high HPN regime as the multiplexing gain (pre-log factor) of the throughput is reduced.

Finally, in the case of different EH profiles, these profiles are generated independently at the TX and the RX, and they are i.i.d with exponential distribution. EH profiles are verified so that they are not similar according to definition 4. EH profiles of the TX and the RX are shown in Fig. 7.

In Fig. 6, energy allocation of OEA algorithm and Similar to Fig. 6, in Fig. 8, the mean HPN at the TX is varied by multiplying the EH profile, while keeping the same shape. As we can see, the heuristic of using OEA approach performs quite well in the different EH profile scenario. Since we could not find a simple algorithm, CVX solver is used to solve the optimization problem [20]. The energy allocation at the TX and the RX is shown in Fig. 9 for the above mentioned policies at an average per frame HPN of

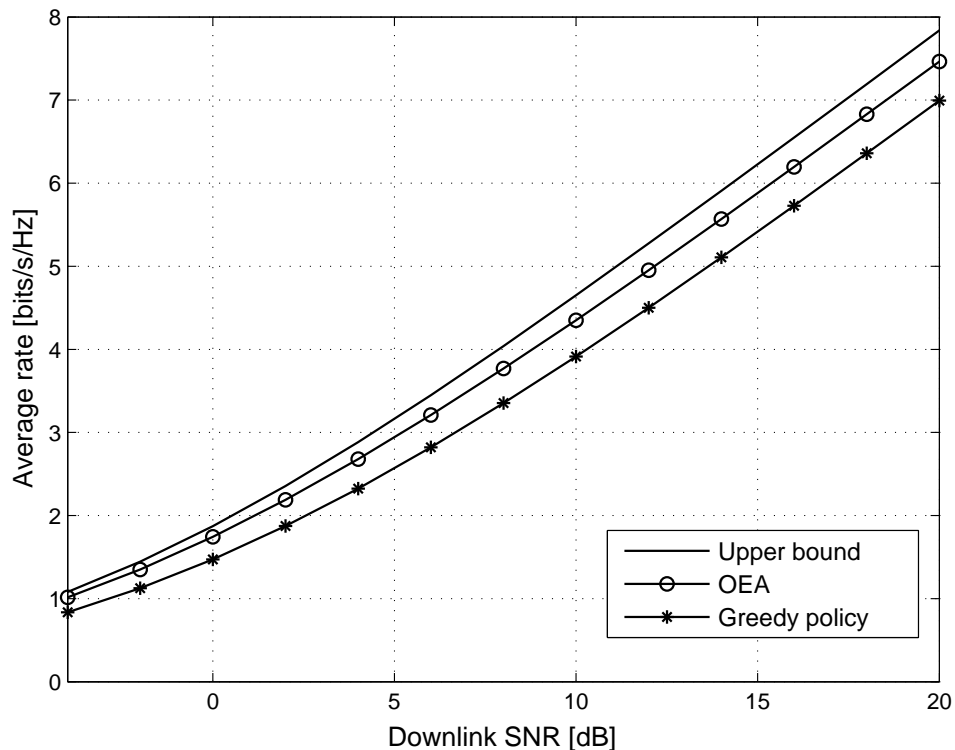


Figure 4. Ergodic rate with EH RX.

0.5 dB at the TX. Different from Fig. 6, the rate scaling with average HPN is same in both the greedy and OEA policies. For the greedy policy, the allocated energy in the EH interval scales with increasing the mean HPN, in contrast to the solar EH profile, where the allocated energy is zero in some intervals.

VII. CONCLUSION

We have studied the problem of feedback design with EH constraints in a point-to-point MISO channel with an EH RX and EH TX. Since the exact expressions of throughput are complicated, concave upper bounds are used in the optimization problems. We first considered the case in which only the RX harvests energy, and optimize the feedback policy. Latter, the general case in which both the TX and the RX harvesting energy is analyzed. We showed that, if EH profiles are similar, the optimization problem can be considerably simplified. We note the result obtained in Proposition 4, with some assumptions, can be used in a general setting that may arise when a concave objective is to be maximized with the EH nodes in a communication network. Numerical results show that the proposed policies not only outperform the

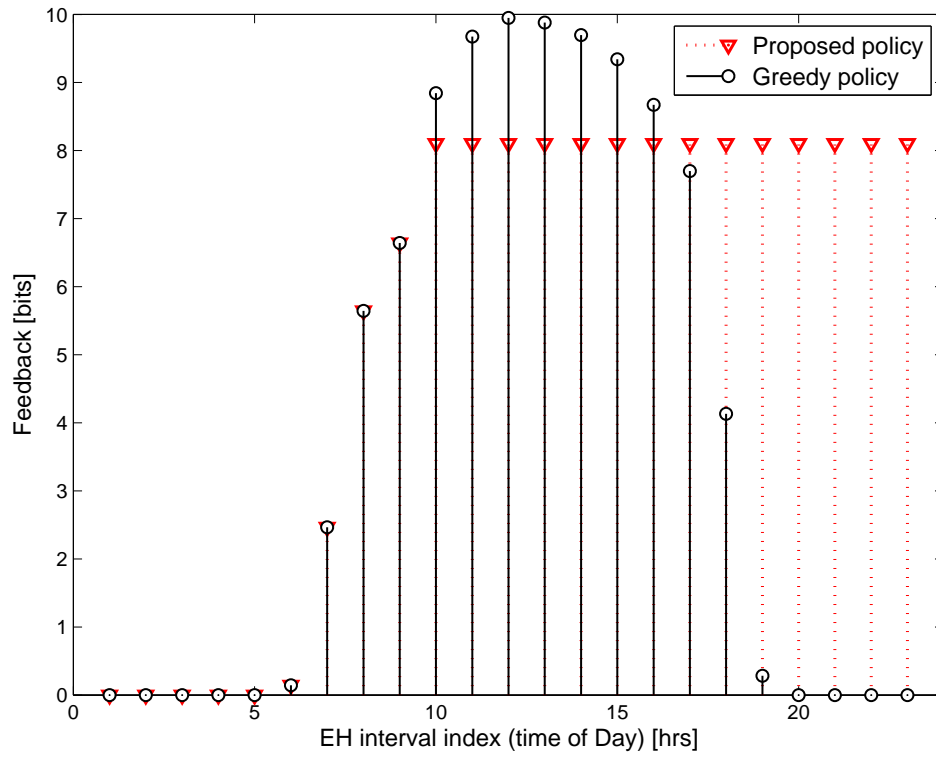


Figure 5. Feedback load at SNR of 10 dB.

greedy policies, but also achieve the performances which are quite close to the upper bound. Finally, we believe that our work sheds light on the design of feedback enabled multi-antenna systems when the nodes depend on EH devices for their energy.

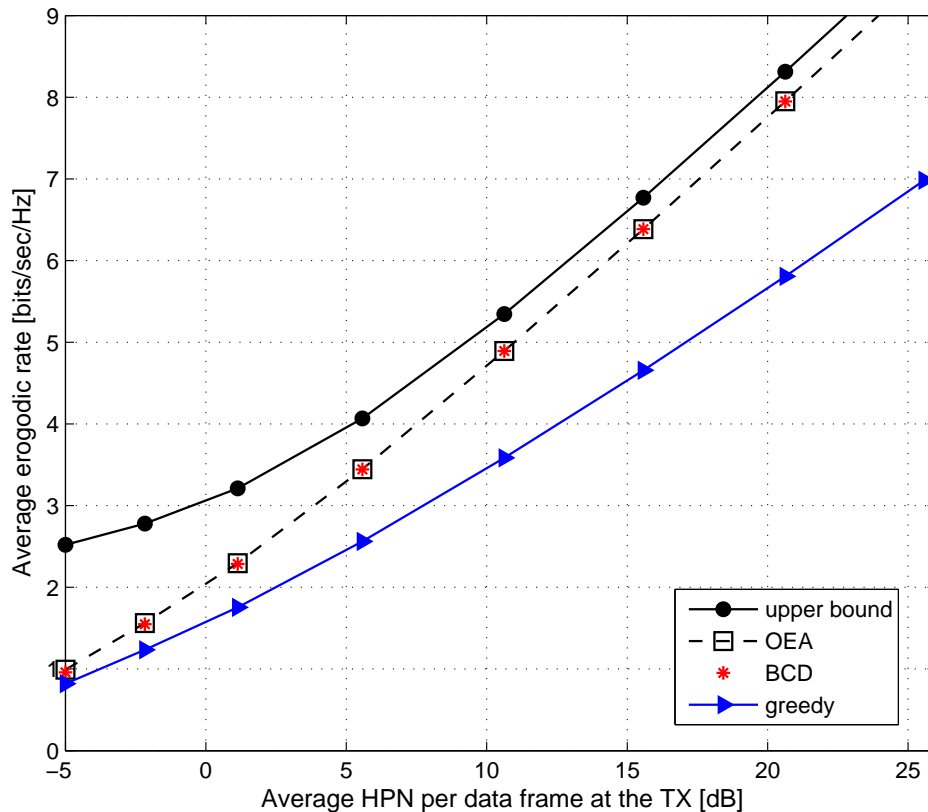


Figure 6. Ergodic rate for similar EH profiles.

APPENDIX

A. Proof of Lemma 1

Let $X_1 = [x_1 \ y_1 \ t_1]^T$, $X_2 = [x_2 \ y_2 \ t_2]^T$, we have

$$\begin{aligned}
 h(\lambda X_1 + (1-\lambda) X_2) &= \Theta g\left(\frac{\lambda y_1 + (1-\lambda) y_2}{\Theta}, \frac{f(\lambda x_1 + (1-\lambda) x_2, \lambda t_1 + (1-\lambda) t_2)}{\Theta}\right) \\
 &\stackrel{(a)}{\geq} \Theta g\left(\frac{\lambda y_1 + (1-\lambda) y_2}{\Theta}, \frac{\lambda f(x_1, t_1) + (1-\lambda) f(x_2, t_2)}{\Theta}\right) \\
 &= \Theta g\left(\frac{\Theta_1}{\Theta} \frac{y_1}{(1-\frac{t_1}{T})} + \frac{\Theta_2}{\Theta} \frac{y_2}{(1-\frac{t_2}{T})}, \frac{\Theta_1}{\Theta} \frac{f(x_1, t_1)}{(1-\frac{t_1}{T})} + \frac{\Theta_2}{\Theta} \frac{f(x_2, t_2)}{(1-\frac{t_2}{T})}\right) \quad (29) \\
 &\stackrel{(b)}{\geq} \Theta_1 g\left(\frac{y_1}{(1-\frac{t_1}{T})}, \frac{f(x_1, t_1)}{(1-\frac{t_1}{T})}\right) + \Theta_2 g\left(\frac{y_2}{(1-\frac{t_2}{T})}, \frac{f(x_2, t_2)}{(1-\frac{t_2}{T})}\right) \\
 &= \lambda h(X_1) + (1-\lambda) h(X_2),
 \end{aligned}$$

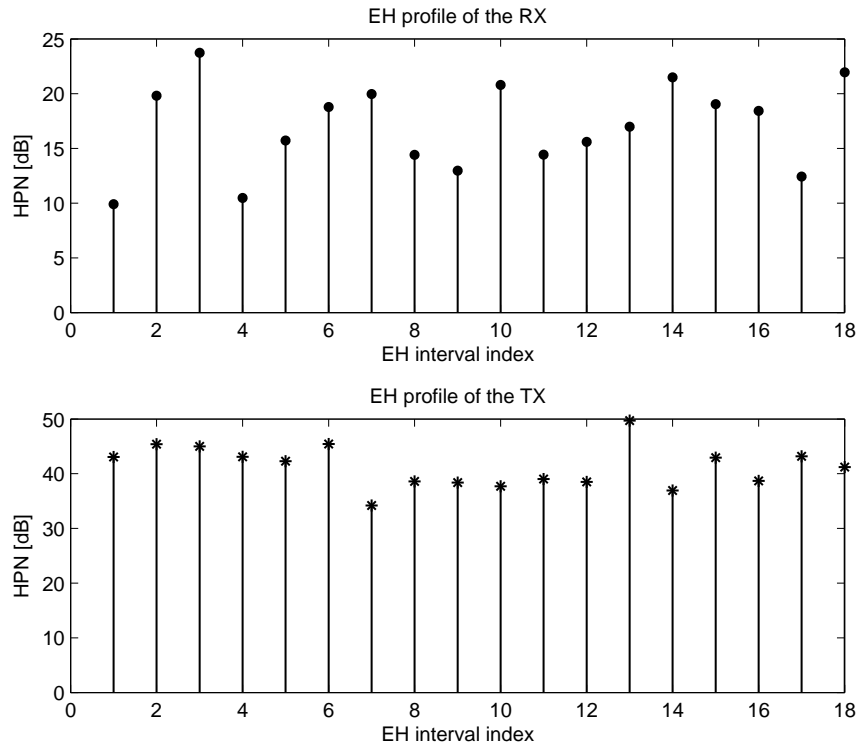


Figure 7. Energy harvesting profiles.

where $\Theta_1 \triangleq \lambda \left(1 - \frac{t_1}{T}\right)$ and $\Theta_2 \triangleq (1 - \lambda) \left(1 - \frac{t_2}{T}\right)$, $\Theta = \Theta_1 + \Theta_2$, and

- (a) follows from the fact that $f(x, t)$ is concave, and $g(y, z)$ is monotonically increasing in each argument.
- (b) follows from the fact that $\frac{\Theta_1}{\Theta} + \frac{\Theta_2}{\Theta} = 1$, and $g(y, z)$ is concave.

B. Proof of Proposition 1

The ergodic rate bound in (8) with $P_k = P, \forall k$ can be written as,

$$R^u(Q_k, \tau_k) = \left(1 - \frac{\tau_k}{T}\right) \log_2 \left(1 + \frac{f(Q_k, \tau_k)}{1 - \frac{\tau_k}{T}}\right), \quad (30)$$

where $f(Q_k, \tau_k) \triangleq PM \left(1 - \frac{M-1}{M} \left(1 + \frac{Q_k}{\tau_k \sigma^2}\right)^{\frac{-\tau_k}{M-1}}\right)$. Since B_k in (3) is concave in Q_k and τ_k , it can be easily seen that $2^{-\frac{B_k}{M-1}} = \left(1 + \frac{Q_k}{\tau_k \sigma^2}\right)^{\frac{-\tau_k}{M-1}}$ is convex, and hence, $f(Q_k, \tau_k)$ is concave. Using Lemma 1 with $g(y, z) = \log_2(1 + z)$ and $f(Q_k, \tau_k)$, we can see that R_k^u is concave. Since the objective function in (9) is the summation of R_k^u 's, it is also concave.

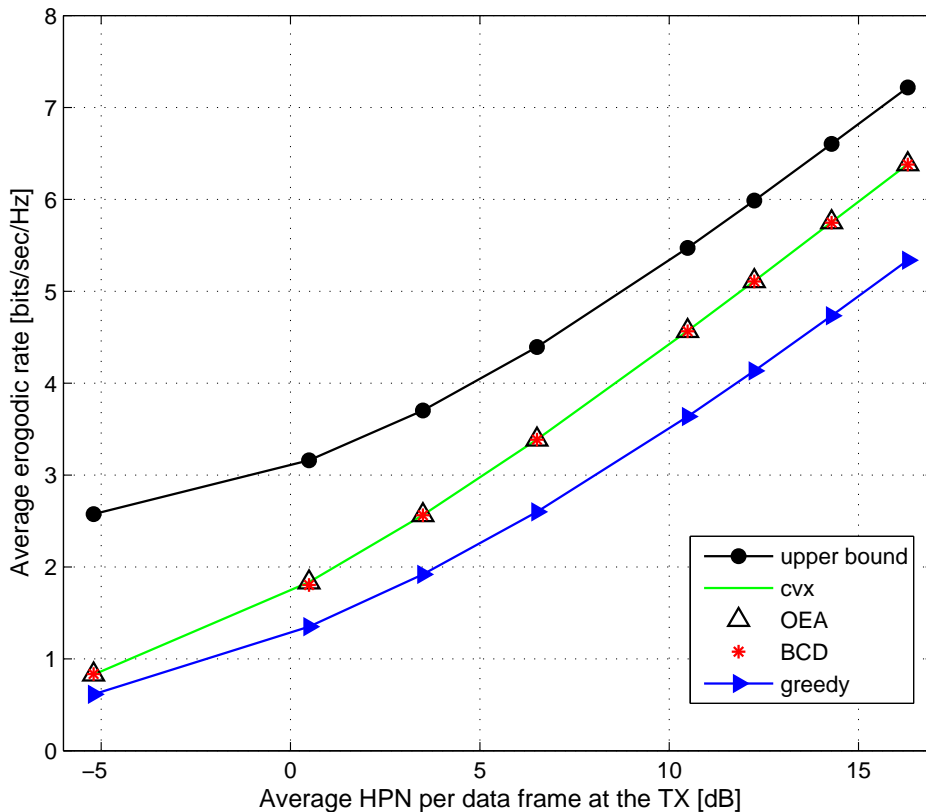


Figure 8. Ergodic rate for different EH profiles.

C. Proof of Proposition 3

First, we show that $g(y, z) = \log(1 + (1 + y)z)$, $(y, z) \in \mathbb{R}_+^2$ is concave for $y \geq 0, z \geq 1$. The Hessian of g is given by

$$\mathbf{J} = \frac{1}{\beta} \begin{pmatrix} -z^2 & 1 \\ 1 & -(1+y)^2 \end{pmatrix}, \quad (31)$$

where $\beta = (1 + (1 + y)z)^2 > 0$. Consider $\mathbf{u}^T \mathbf{J} \mathbf{u} = -\frac{1}{\beta} (a^2 z^2 + b^2 (1 + y)^2 - 2ab)$, where $\mathbf{u} = [a \ b]^T \in \mathbb{R}^2$. It can be easily seen that $\mathbf{u}^T \mathbf{J} \mathbf{u} \leq 0$ for $ab \leq 0$. For $ab > 0$, since $z(1 + y) \geq 1$, $\mathbf{u}^T \mathbf{J} \mathbf{u} = -\frac{1}{\beta} [(az - b(1 + y))^2 + 2ab(z(1 + y) - 1)] \leq 0$. As Hessian is negative semidefinite, $g(y, z)$ is concave.

Reproducing the ergodic rate bound in (18),

$$R^{ub}(Q_k, \tau_k) = \left(1 - \frac{\tau_k}{T}\right) \log_2 \left(1 + \left(1 + \frac{P_k}{1 - \frac{\tau_k}{T}}\right) \frac{f(Q_k, \tau_k)}{1 - \frac{\tau_k}{T}}\right), \quad (32)$$

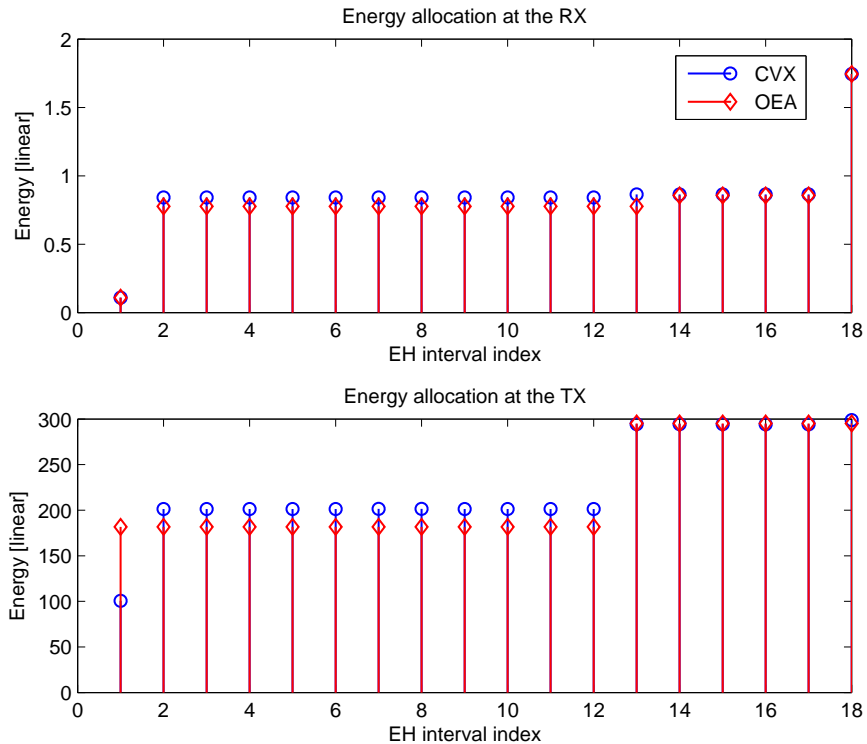


Figure 9. Energy allocation at the TX and the RX.

where $f(Q_k, \tau_k) \triangleq M - (M - 1) \left(1 + \frac{Q_k}{\tau_k \sigma^2}\right)^{\frac{-\tau_k}{M-1}}$. Since B_k in (3) is concave in Q_k and τ_k , it can be easily seen that $2^{-\frac{B_k}{M-1}} = \left(1 + \frac{Q_k}{\tau_k \sigma^2}\right)^{\frac{-\tau_k}{M-1}}$ is convex, and hence, $f(Q_k, \tau_k)$ is concave. Using Lemma 1 with $g(y, z) = \log(1 + (1 + y)z)$ and $f(Q_k, \tau_k)$, we can see that R_k^{ub} is concave. Since the objective function in (22) is the summation of R_k^{ub} 's, it is also concave.

D. Proof of Proposition 4

First, $(\mathbf{P}^*, \mathbf{Q}^*)$ is shown to be the solution of (27) and then $\boldsymbol{\tau}^*$ is obtained by (28). Before solving (27), we prove that

$$(\mathbf{P}^*, \mathbf{Q}^*) = \arg \max_{g, P_k, Q_k} \sum_{k=1}^K g(P_k, Q_k) \quad \text{s.t. } \forall k, (P_k, Q_k) \in \tilde{\mathfrak{J}}, g \in \mathfrak{C}, \quad (33)$$

where \mathfrak{C} is the set of all continuous concave functions. Since (27) is a special case of (33), $(\mathbf{P}^*, \mathbf{Q}^*)$ is also the solution of (27).

Before starting, we note that the notations and properties of the OEA algorithm discussed in Sec IV-A are used throughout the proof. By contradiction, let us assume that there exists a $[\hat{\mathbf{P}}^T \ \hat{\mathbf{Q}}^T]^T \neq [\mathbf{P}^{*T} \ \mathbf{Q}^{*T}]^T$ and $(\hat{\mathbf{P}}, \hat{\mathbf{Q}})$ be the solution of (33). Then, by Theorem 2 we have,

$$\left[\hat{\mathbf{P}}^T \ \hat{\mathbf{Q}}^T \right]^T \preceq \left[\mathbf{P}^T \ \mathbf{Q}^T \right]^T, \quad \forall (\mathbf{P}, \mathbf{Q}) \in \tilde{\mathfrak{J}}. \quad (34)$$

Since $(\mathbf{P}^*, \mathbf{Q}^*) \in \tilde{\mathfrak{J}}$, by (34) and Definition 3,

$$\left[\hat{\mathbf{P}}^T \ \hat{\mathbf{Q}}^T \right]^T = \left[\mathbf{P}^{*T} \ \mathbf{Q}^{*T} \right]^T \mathbf{D}. \quad (35)$$

By feasibility (22b),

$$\sum_{j=t_{i-1}+1}^{t_i} \hat{Q}_j \leq V_i = \sum_{j=t_{i-1}+1}^{t_i} E_j^r / L. \quad (36)$$

Applying (36) at $i = 1$,

$$\sum_{j=1}^{t_1} \hat{Q}_j = \sum_{j=1}^{t_1} \sum_{i=1}^K Q_i^* \{\mathbf{D}\}_{i,j} \leq V_1. \quad (37)$$

By (P1) and (P2), $Q_i^* = Q_{(1)}^* + L_i$, where

$$\begin{aligned} L_i &= 0 \quad \forall i \in [1 : t_1], \\ L_i &> 0 \quad \forall i \in [t_1 + 1 : K]. \end{aligned} \quad (38)$$

From (37) and (38)

$$\sum_{j=1}^{t_1} \sum_{i=1}^K Q_{(1)}^* \{\mathbf{D}\}_{i,j} + \sum_{j=1}^{t_1} \sum_{i=t_1+1}^K L_i \{\mathbf{D}\}_{i,j} \leq V_1. \quad (39)$$

Using the fact that \mathbf{D} is doubly stochastic and by (P1), $t_1 Q_{(1)}^* = V_1$, in (39)

$$\sum_{j=1}^{t_1} \sum_{i=t_1+1}^K L_i \{\mathbf{D}\}_{i,j} \leq 0, \quad L_i > 0. \quad (40)$$

From (40),

$$\{\mathbf{D}\}_{i,j} = 0, \quad \forall i \in [t_1 + 1 : K], \quad \forall j \in [1 : t_1]. \quad (41)$$

As \mathbf{D} is doubly stochastic, using (P1) and (41),

$$\hat{Q}_j = \sum_{i=1}^{t_1} Q_{(1)}^* \{\mathbf{D}\}_{i,j} = Q_{(1)}^* = Q_j^*, \quad \forall j \in [1 : t_1]. \quad (42)$$

Since \mathbf{D} double stochastic and using (41),

$$\begin{aligned} \sum_{i=1}^{t_1} \sum_{j=1}^K \{\mathbf{D}\}_{i,j} &= t_1, \\ \sum_{i=1}^{t_1} \{\mathbf{D}\}_{i,j} &= 1, \quad \forall j \in [1 : t_1]. \end{aligned} \quad (43)$$

Using (43),

$$\sum_{i=1}^{t_1} \sum_{j=1}^K \{\mathbf{D}\}_{i,j} = \sum_{i=1}^{t_1} \sum_{j=1}^{t_1} \{\mathbf{D}\}_{i,j} + \sum_{i=1}^{t_1} \sum_{j=t_1+1}^K \{\mathbf{D}\}_{i,j}, \quad (44)$$

From (44), we can see that

$$\sum_{i=1}^{t_1} \sum_{j=t_1+1}^K \{\mathbf{D}\}_{i,j} = 0, \quad (45)$$

hence,

$$\{\mathbf{D}\}_{i,j} = 0, \quad \forall i \in [1 : t_1], \forall j \in [t_1 + 1 : K]. \quad (46)$$

Applying (36) at $i = 2$,

$$\sum_{j=t_1+1}^{t_2} \hat{Q}_j = \sum_{j=t_1+1}^{t_2} \sum_{i=1}^K Q_i^* \{\mathbf{D}\}_{i,j} \leq V_2. \quad (47)$$

By (P1) and (P2), $Q_i^* = Q_{(2)}^* + L_i$, where

$$\begin{aligned} L_i &< 0 \quad \forall i \in [1 : t_1], \\ L_i &= 0 \quad \forall i \in [t_1 + 1 : t_2], \\ L_i &> 0 \quad \forall i \in [t_2 + 1 : K]. \end{aligned} \quad (48)$$

From (47) and (48),

$$\sum_{j=t_1+1}^{t_2} \sum_{i=1}^K L_i \{\mathbf{D}\}_{i,j} + \sum_{j=t_1+1}^{t_2} \sum_{i=1}^K Q_{(2)}^* \{\mathbf{D}\}_{i,j} \leq V_2. \quad (49)$$

Since \mathbf{D} is doubly stochastic, by (P1), $(t_2 - t_1) Q_{(2)}^* = V_2$, and using (46), (48) in (49),

$$\sum_{j=t_1+1}^{t_2} \sum_{i=t_2+1}^K L_i \{\mathbf{D}\}_{i,j} \leq 0, L_i > 0. \quad (50)$$

From (50),

$$\{\mathbf{D}\}_{i,j} = 0, \quad \forall i \in [t_2 + 1 : K], \forall j \in [t_1 + 1 : t_2]. \quad (51)$$

As \mathbf{D} is doubly stochastic, using (P1), (46) and (51),

$$\hat{Q}_j = Q_{(2)}^* \sum_{i=t_1+1}^{t_2} \{\mathbf{D}\}_{i,j} = Q_{(2)}^* = Q_j^*, \forall j \in [t_1 + 1 : t_2]. \quad (52)$$

Since \mathbf{D} is doubly stochastic, using (46) and (51),

$$\begin{aligned} \sum_{i=t_1+1}^{t_2} \sum_{j=1}^K \{\mathbf{D}\}_{i,j} &= t_2 - t_1, \\ \sum_{i=t_1+1}^{t_2} \{\mathbf{D}\}_{i,j} &= 1, \quad \forall j \in [t_1 + 1 : t_2]. \end{aligned} \quad (53)$$

Using (53),

$$\sum_{i=t_1+1}^{t_2} \sum_{j=1}^K \{\mathbf{D}\}_{i,j} = \sum_{i=t_1+1}^{t_2} \sum_{j=t_1+1}^{t_2} \{\mathbf{D}\}_{i,j} + \sum_{i=t_1+1}^{t_2} \sum_{j=t_2+1}^K \{\mathbf{D}\}_{i,j}, \quad (54)$$

From (54) we can see that

$$\sum_{i=t_1+1}^{t_2} \sum_{j=t_2+1}^K \{\mathbf{D}\}_{i,j} = 0, \quad (55)$$

hence,

$$\{\mathbf{D}\}_{i,j} = 0, \forall i \in [t_1 + 1 : t_2] \text{ and } \forall j \in [t_2 + 1 : K]. \quad (56)$$

Continuing this approach for $i = 3, \dots, (|S| - 1)$, we get $\hat{\mathbf{Q}} = \mathbf{Q}^*$. Since the EH profiles are similar, replacing $\hat{\mathbf{Q}}$ by $\hat{\mathbf{P}}$ and E_j^r by E_j^t/T in the above proof, we reach similar conclusion for $\hat{\mathbf{P}}$ i.e., $\hat{\mathbf{P}} = \mathbf{P}^*$. Therefore, $[\hat{\mathbf{P}}^T \hat{\mathbf{Q}}^T]^T = [\mathbf{P}^{*T} \mathbf{Q}^{*T}]^T$.

E. Proof of Lemma 2

Assuming that at least one of the P_k, Q_k is not monotonically increasing in k . Without loss of generality (w.l.o.s) we consider the cases where $P_k > P_{k+1}, Q_k \geq Q_{k+1}$ and $P_k < P_{k+1}, Q_k > Q_{k+1}$. In the case of $P_k > P_{k+1}, Q_k \geq Q_{k+1}$, we can construct a new feasible policy,

$$\begin{aligned} P'_k &= P'_{k+1} = \frac{P_k + P_{k+1}}{2}, \\ Q'_k &= Q'_{k+1} = \frac{Q_k + Q_{k+1}}{2}. \end{aligned} \quad (57)$$

Since the objective function is concave, by Jensen's inequality, the new policy strictly increases the objective. Finally considering the case where $P_k < P_{k+1}, Q_k > Q_{k+1}$, we can construct another feasible policy,

$$\begin{aligned} P'_k &= P_k, \quad P'_{k+1} = P_{k+1}, \\ Q'_k &= Q_{k+1}, \quad Q'_{k+1} = Q_k. \end{aligned} \quad (58)$$

The function R^{ub} with variables P, Q, τ can be written as,

$$R^{ub}(P, Q, \tau) = t \log_2 \left(1 + \left(\frac{1}{t} + \frac{P}{t^2} \right) f \right), \quad (59)$$

where $f \triangleq M - (M - 1) \left(1 + \frac{Q}{\tau \sigma^2} \right)^{\frac{-\tau}{M-1}}$, $t \triangleq 1 - \frac{\tau}{T}$ and $0 \leq \tau < T$. The second order partial derivative of $R^{ub}(P, Q, \tau)$ is given by,

$$\frac{\partial^2 R^{ub}}{\partial P \partial Q} = \frac{\frac{\partial f}{\partial Q}}{t(1 + f/t + Pf/t^2)^2}. \quad (60)$$

Since f is monotonic in Q , (60) is positive. As $\frac{\partial^2 R^{ub}}{\partial P \partial Q} > 0$, by the definition of derivative,

$$R^{ub}(P, Q, \tau) + R^{ub}(P + \delta, Q + \alpha, \tau) > R^{ub}(P + \delta, Q, \tau) + R^{ub}(P, Q + \alpha, \tau), \quad \delta, \alpha > 0. \quad (61)$$

Since (61) holds $\forall 0 \leq \tau < T$, we have

$$\tilde{R}^{ub}(P, Q) + \tilde{R}^{ub}(P + \delta, Q + \alpha) > \tilde{R}^{ub}(P + \delta, Q) + \tilde{R}^{ub}(P, Q + \alpha), \quad (62)$$

where \tilde{R}^{ub} is obtained by,

$$\tilde{R}^{ub}(P, Q) = \max_{\tau} R^{ub}(P, Q, \tau). \quad (63)$$

From (62) and (58),

$$\tilde{R}^{ub}(P'_k, Q'_k) + \tilde{R}^{ub}(P'_{k+1}, Q'_{k+1}) > \tilde{R}^{ub}(P_k, Q_k) + \tilde{R}^{ub}(P_{k+1}, Q_{k+1}). \quad (64)$$

F. Proof of Lemma 3

Let us assume that the transmission rates in the k -th and $k+1$ -th intervals are different, i.e., $\tilde{R}^{ub}(P_k, Q_k) \neq \tilde{R}^{ub}(P_{k+1}, Q_{k+1})$. Before the $k+1$ -th interval, the energy in the buffers of TX and the RX are $\Delta_r \triangleq \sum_{i=1}^k E_i^r - L \sum_{i=1}^k Q_i$ and $\Delta_t \triangleq \sum_{i=1}^k E_i^t - LT \sum_{i=1}^k P_i$, respectively. W.l.o.s, we assume that $\Delta_r \leq \Delta_t$. We can construct another feasible policy

$$\begin{aligned} P'_k &= P_k + \delta, & P'_{k+1} &= P_{k+1} - \delta, \\ Q'_k &= Q_k + \delta, & Q'_{k+1} &= Q_{k+1} - \delta, \end{aligned} \quad (65)$$

where δ is chosen such that $\delta < \Delta_r$ and $Q'_k < Q'_{k+1}$. Now, (65) can be written as

$$\begin{aligned} P'_k &= \alpha P_k + (1 - \alpha) P_{k+1}, & P'_{k+1} &= (1 - \alpha) P_k + \alpha P_{k+1}, \\ Q'_k &= \alpha Q_k + (1 - \alpha) Q_{k+1}, & Q'_{k+1} &= (1 - \alpha) Q_k + \alpha Q_{k+1}, \end{aligned} \quad (66)$$

where $\alpha = 1 - \delta / (Q_{k+1} - Q_k)$. From (66) and Jensen's inequality,

$$\tilde{R}^{ub}(P'_k, Q'_k) + \tilde{R}^{ub}(P'_{k+1}, Q'_{k+1}) \geq \tilde{R}^{ub}(P_k, Q_k) + \tilde{R}^{ub}(P_{k+1}, Q_{k+1}). \quad (67)$$

REFERENCES

- [1] R. Gangula, D. Gesbert, and D. Gunduz, "Optimizing feedback in energy harvesting MISO communication channels," in *IEEE GlobalSIP*, Dec 2013.
- [2] A. Kansal, J. Hsu, S. Zahedi, and M. B. Srivastava, "Power management in energy harvesting sensor networks," *ACM Trans. Embed. Comput. Syst.*, vol. 6, no. 4, Sep. 2007.
- [3] S. Sudevalayam and P. Kulkarni, "Energy harvesting sensor nodes: survey and implications," *IEEE Communications Surveys Tutorials*, vol. 13, no. 3, pp. 443–461, 2011.
- [4] O. Ozel, K. Tutuncuoglu, J. Yang, S. Ulukus, and A. Yener, "Transmission with energy harvesting nodes in fading wireless channels: optimal policies," *IEEE JSAC*, vol. 29, no. 8, pp. 1732–1743, 2011.
- [5] M. Antepi, E. Uysal-Biyikoglu, and H. Erkal, "Optimal packet scheduling on an energy harvesting broadcast link," *IEEE JSAC*, vol. 29, no. 8, pp. 1721–1731, 2011.

- [6] J. Yang, O. Ozel, and S. Ulukus, "Broadcasting with an energy harvesting rechargeable transmitter," *IEEE Transactions on Wireless Communications*, vol. 11, no. 2, pp. 571–583, 2012.
- [7] B. Devillers and D. Gunduz, "A general framework for the optimization of energy harvesting communication systems with battery imperfections," *Journal of Comm. and Nets*, vol. 14, no. 2, pp. 130–139, 2012.
- [8] D. Gunduz and B. Devillers, "Two-hop communication with energy harvesting," in *CAMSAP*, 2011.
- [9] O. Orhan and E. Erkip, "Optimal transmission policies for energy harvesting two-hop networks," in *CISS*, 2012.
- [10] C. Huang, R. Zhang, and S. Cui, "Throughput maximization for the gaussian relay channel with energy harvesting constraints," *IEEE Journal on Selected Areas in Communications*, vol. 31, no. 8, pp. 1469–1479, August 2013.
- [11] M. Gregori and M. Payaro, "Throughput maximization for a wireless energy harvesting node considering the circuitry power consumption," in *IEEE VTC Fall*, Sept 2012.
- [12] O. Orhan, D. Gunduz, and E. Erkip, "Optimal packet scheduling for an energy harvesting transmitter with processing cost," in *IEEE ICC*, June 2013, pp. 3110–3114.
- [13] D. Gunduz, K. Stamatiou, N. Michelusi, and M. Zorzi, "Designing intelligent energy harvesting communication systems," *IEEE Communications Magazine*, vol. 52, no. 1, pp. 210–216, January 2014.
- [14] D. Love, R. Heath, V. K. N. Lau, D. Gesbert, B. Rao, and M. Andrews, "An overview of limited feedback in wireless communication systems," *IEEE JSAC*, vol. 26, no. 8, pp. 1341–1365, 2008.
- [15] A. W. Marshall, I. Olkin, and B. C. Arnold, *Inequalities: Theory of majorization and its applications*. Springer, 2010.
- [16] W. Santipach and M. Honig, "Optimization of training and feedback overhead for beamforming over block fading channels," *IEEE Transactions on Information Theory*, vol. 56, no. 12, pp. 6103–6115, Dec 2010.
- [17] M. Kobayashi, N. Jindal, and G. Caire, "Training and feedback optimization for multiuser MIMO downlink," *IEEE Transactions on Communications*, vol. 59, no. 8, pp. 2228–2240, 2011.
- [18] C. K. Au-Yeung and D. Love, "On the performance of random vector quantization limited feedback beamforming in a MISO system," *IEEE Transactions on Wireless Comm*, vol. 6, no. 2, pp. 458–462, 2007.
- [19] N. Jindal, "MIMO broadcast channels with finite-rate feedback," *IEEE Trans on Inf. Theory*, vol. 52, no. 11, pp. 5045–5060, 2006.
- [20] S. Boyd and L. Vandenberghe, *Convex optimization*. New York, NY, USA: Cambridge University Press, 2004.
- [21] C. K. Ho and R. Zhang, "Optimal energy allocation for wireless communications with energy harvesting constraints," *IEEE Transactions on Signal Processing*, vol. 60, no. 9, pp. 4808–4818, 2012.
- [22] M. A. Zafer and E. Modiano, "A calculus approach to energy-efficient data transmission with quality-of-service constraints," *IEEE/ACM Trans. Netw.*, vol. 17, no. 3, pp. 898–911, Jun. 2009.
- [23] O. Ozel and S. Ulukus, "Achieving AWGN capacity under stochastic energy harvesting," *IEEE Trans on Inf. Theory*, vol. 58, no. 10, pp. 6471–6483, 2012.
- [24] D. Bertsekas, *Nonlinear programming*. Athena Scientific, 1999.
- [25] S. Reddy and C. Murthy, "Dual-stage power management algorithms for energy harvesting sensors," *IEEE Trans on Wireless Comm*, vol. 11, no. 4, pp. 1434–1445, 2012.
- [26] "Solar Resource and Meteorological Assessment Project (SOLRMAP)," <http://www.nrel.gov/midc/lmu/>.